

A second order constitutive theory for polyatomic gases: theory and applications

Anirudh S. Rana¹†, and Sukratu Barve²

¹Department of Mathematics, BITS Pilani, Pilani Campus, Rajasthan 333031, India

²Department of Scientific Computing, Modeling and Simulation, Savitribai Phule Pune University, Pune 411007, India

(Received xx; revised xx; accepted xx)

In the classical irreversible thermodynamics (CIT) framework, the Navier-Stokes-Fourier (NSF) constitutive equations are obtained so as they satisfy the entropy inequality, by and large assuming that the entropy flux is equal to the heat flux over the temperature. This article is focused on the derivation of second-order constitutive equations for polyatomic gases; it takes the basis of CIT, but most importantly, allowing up to quadratic nonlinearities in the entropy flux. Mathematical similarities between the proposed model and the classic Stokes-Laplace equations are exploited so as to construct analytic/semi-analytic solutions for the slow rarefied gas flow over different shapes. A set of second-order boundary conditions are formulated such that the model's prediction for the drag force is in excellent agreement with the experimental data over the whole range of Knudsen number. We have also computed the normal shock structure in nitrogen for Mach $Ma \lesssim 4$. A very good agreement was observed with the kinetic theory, as well as with the experimental data.

1. Introduction

The gas most commonly encountered in everyday life is air. It is a mixture of polyatomic gases—primarily nitrogen, which constitutes about 78% of air, and oxygen at about 21% along with trace amount of constituents, such as argon, carbon dioxide, ozone, and water vapor; most of these are polyatomic gases. Air also contains tiny particles called aerosols, such as fog, dust, smoke and particulate air pollutants, so called respirable ultrafine particulates (UFPs). Owing to their nanoscale size, UFPs can penetrate deep into the lungs, blood streams and can have severe health implications including heart attacks and respiratory diseases (De Falco *et al.* 2017). Aerosols can also be produced by coughing or sneezing and airborne viruses can pass from person to person through these nanoscale droplets; therefore, scientists have paid much attention to dynamics of aerosols that waft through the air.

Modeling of micro/nano gas flows is especially intriguing because classical gas dynamics models fail to capture the flow characteristics (such as, drag force on aerosols, mass and heat flux on the evaporation meniscus) in rarefied conditions. As the representative physical length scale (L) of the flow becomes comparable to the mean free path (λ) in the gas, i.e., the Knudsen number Kn ($= \lambda/L$) ≈ 1 , Navier-Stokes-Fourier (NSF) equations fail to predict thermal and fluid flow fields to sufficient accuracy. The Boltzmann equation (Kremer 2010) in such a situation offers a more accurate description of the micro/nano gas flows, but unfortunately is computationally expensive. As a work around over the last few years, an impressive body of research has been devoted to the development of extended hydrodynamic models for polyatomic gases (Zhdanov 1968; Mallinger 1998; Kremer 2010; Cai & Li 2014; Rahimi & Struchtrup 2014), which may provide accurate and computationally efficient simulation-for-design capabilities down to nanoscales.

The notion of extended hydrodynamic models goes back to Grad's pioneering work on

† Email address for correspondence: anirudh.rana@pilani.bits-pilani.ac.in

approximating the Boltzmann equation via moment equations (Grad 1958). The 13 moment equations obtained via Grad’s method yield unphysical sub-shocks and also prone to loose their hyperbolicity in strong non-equilibrium conditions. Struchtrup & Torrilhon (2003; 2004) developed a linearly stable system of regularized 13 moment (R13) equations for monoatomic gases using the order-of-magnitude method (Struchtrup 2005) by combining the ideas of the Chapman–Enskog (Chapman & Cowling 1970) and Grad’s methods. The regularization process extends the validity of the Grad closures through the addition of higher-order derivatives and provides smooth shock structures. Rahimi & Struchtrup (2014) using the same method obtained a hierarchy of moment equations for polyatomic gases at different levels of accuracy. Cai & Li (2014) proposed a numerical regularized moment method of arbitrary order (NRxx) for polyatomic gases with ES-BGK collision operator.

Unfortunately, the extended hydrodynamic equations obtained by Grad’s method, the Chapman–Enskog method or the order-of-magnitude method are not accompanied by a proper entropy balance with strictly non-negative production. This might lead to breakdown of solutions or unphysical results (Struchtrup & Nadler 2020). Another approach towards approximation of the Boltzmann equation is rational extended thermodynamics (RET) framework (Müller & Ruggeri 2013; Ruggeri & Sugiyama 2015), which, however, has the same limitation as those for the moment equations (only the linearized equations have a proper entropy law) Another popular family of moment closure methods is the maximum-entropy hierarchy (Junk & Unterreiter 2002; Torrilhon 2016). The maximum-entropy closures ensure entropy inequality and hyperbolicity but they suffer from high computational cost incurred to compute the closure. Furthermore, it is impossible to obtain a closed form solution from the higher order maximum-entropy closures.

Recently, a phenomenological procedure for monoatomic gases was proposed (Rana *et al.* 2018) in which the entropy flux contains additional nonlinear contributions in stress and heat flux—an ansatz consistent with the RET. The resulting coupled constitutive relations (CCR) are accompanied by an entropy inequality, in which the entropy remains the equilibrium entropy as integrated from the equilibrium Gibbs equation, but entropy flux and entropy generation exhibit higher order correction terms. These additional terms in the entropy flux add a few second order correction terms to the NSF system. The CCR system allows to formulate thermodynamically consistent boundary conditions and their efficacy in capturing rarefaction effects at small scales was shown by Rana *et al.* (2018, 2021*b*). In this work, we extend the theory of the coupled constitutive relations to polyatomic gases. The resulting model (polyatomic-CCR) is benchmarked with experimental data for the slow rarefied gas flow over different shapes; the model’s prediction for the drag force is in excellent agreement with the experiments. The normal shocks structure in nitrogen is also computed for the Mach number $Ma \lesssim 4$; again, there is a good match between the polyatomic-CCR model and the experiments. In large measures, the polyatomic-CCR model enables the study of small-scale physics that is not accessible by the conventional fluid dynamics at a very little to no added computational cost.

The remainder of this paper is organized as follows. In Section 2, we introduce the governing equations and CIT framework. In Section 2.3, derivation of the polyatomic-CCR model is presented. In Section 3, we introduce linearized and dimensionless equations followed by their solutions for slow rarefied gas flow over a spherical and doublet particle in Section 4 and 6, respectively. A brief derivation of the Green’s functions is also given in Section 5. In Section 6, normal shock structure in nitrogen gas is computed. We conclude and discuss future directions in Section 7.

2. The governing equations

2.1. Conservation laws for polyatomic gases

The conservation laws are the balance equations for the mass density ρ , the fluid velocity \mathbf{v} , internal energy u . For a compressible, polyatomic gas these are formulated as (Kremer 2010)

$$\frac{\partial \rho}{\partial t} + \nabla \cdot (\rho \mathbf{v}) = 0, \quad (2.1a)$$

$$\frac{\partial (\rho \mathbf{v})}{\partial t} + \nabla \cdot [\rho \mathbf{v} \otimes \mathbf{v} + (p + \Pi) \mathbf{I} + \boldsymbol{\sigma}] = 0, \quad (2.1b)$$

$$\frac{\partial \left(\rho u + \frac{1}{2} \rho v^2 \right)}{\partial t} + \nabla \cdot \left[\left(\rho u + \frac{1}{2} \rho v^2 + p + \Pi \right) \mathbf{v} + \boldsymbol{\sigma} \cdot \mathbf{v} + \mathbf{q} \right] = 0, \quad (2.1c)$$

where p is the pressure, Π is the dynamic pressure, $\boldsymbol{\sigma}$ is the symmetric and trace free part of the pressure tensor and \mathbf{q} is the heat flux. The internal energy u , of a polyatomic ideal gas is related to the thermodynamics temperature T through the Caloric equation $du = \frac{3+\delta}{2} d\theta := \frac{d\theta}{\gamma-1}$, i.e., the constant volume specific heat is given by $c_v = \frac{3+\delta}{2} R$. Here, R is the ideal gas constant and γ ($= c_p/c_v$) is the specific heat ratio.

For convenience, we also define the temperature and the dynamic temperature in energy units as $\theta := RT$ and $\vartheta := \Pi/\rho$. A value δ can be chosen such that the proper caloric equation of gas is recovered, i.e.,

$$\delta = \frac{5 - 3\gamma}{\gamma - 1}. \quad (2.2)$$

For example, for the nitrogen gas or for the dry air $\gamma \approx 1.4$, which gives $\delta = 2$.

In molecular gases, c_v depends on the temperature, which implies δ should also be a function of temperature. However, for processes where changes in the temperature are small, one can assume c_v to be constant, hence, δ can be assumed constant. Throughout, this article we consider such processes, and assume δ to be constant. Furthermore, the pressure p in (2.1) is assumed to given by the ideal gas law, $p = \rho\theta$.

The conservation laws (2.1) need to be closed by constitutive relations between the field variables (ρ , \mathbf{v} and θ) and their fluxes (Π , $\boldsymbol{\sigma}$ and \mathbf{q}). These constitutive relations can be obtained by enforcing the second law inequality, as shown below.

2.2. NSF constitutive relations from the CIT framework

The CIT framework is based on the hypothesis of local equilibrium, according to which, the Gibbs relation is assumed to be locally valid, i.e.,

$$\theta d\eta = du - \frac{p}{\rho^2} d\rho \quad (2.3)$$

where $\eta = s/R$ denotes the dimensionless entropy (s being the dimensional entropy). Multiplying the last equation with ρ , and replacing $D\rho/Dt$, and Du/Dt by means of the conservation laws (2.1), one obtains the entropy balance equation as

$$\frac{\partial (\rho\eta)}{\partial t} + \nabla \cdot \left[\rho\eta\mathbf{v} + \frac{\mathbf{q}}{\theta} \right] = -\frac{1}{\theta} \Pi \nabla \cdot \mathbf{v} - \frac{1}{\theta} \boldsymbol{\sigma} : \langle \nabla \mathbf{v} \rangle - \frac{\mathbf{q}}{\theta^2} \cdot \nabla \theta. \quad (2.4)$$

Here, the angular parentheses around a matrix denotes the symmetric and trace-free part, i.e., $\langle A \rangle = (A + A^T)/2 - \mathbf{I} \text{Tr}(A)/3$; \mathbf{I} being the identity matrix and $\text{Tr}(A)$ is the trace of A .

Comparing (2.4) with a general balance equation of the form

$$\partial (\rho\eta) / \partial t + \nabla \cdot (\rho\eta\mathbf{v} + \boldsymbol{\Psi}) = \Sigma, \quad (2.5)$$

it follows that the non-convective entropy flux $\Psi = \mathbf{q}/\theta$ and the entropy production

$$\Sigma = -\frac{1}{\theta}\Pi\underline{\nabla \cdot \mathbf{v}} - \frac{1}{\theta}\sigma : \langle \underline{\nabla \mathbf{v}} \rangle - \frac{\mathbf{q}}{\theta^2} \cdot \underline{\nabla \theta}. \quad (2.6)$$

The expression for Σ forms a bi-linear relationship in the thermodynamic fluxes (Π , σ , \mathbf{q}) and the underlined thermodynamic forces. To guarantee the positiveness of the entropy production Σ , it is sufficient to assume linear flux-force relations of the form

$$\sigma = -2\mu \langle \underline{\nabla \mathbf{v}} \rangle, \Pi = -\mu_b \underline{\nabla \cdot \mathbf{v}} \quad \text{and} \quad \mathbf{q} = -\kappa \underline{\nabla \theta}, \quad (2.7)$$

where μ , μ_b and κ/R are positive phenomenological coefficients, identified as the viscosity, the bulk viscosity and the thermal conductivity of the gas, respectively.

2.3. Coupled Constitutive Relations from the Gibbs relation

To obtain second-order coupled constitutive relations, the entropy flux Ψ entails all the quadratic vector terms in \mathbf{q} , σ , and Π , i.e.,

$$\Psi = \frac{\mathbf{q}}{\theta} - \alpha_0 \frac{\sigma \cdot \mathbf{q}}{p\theta} - \beta_0 \frac{\Pi \mathbf{q}}{p\theta}, \quad (2.8)$$

where α_0 , β_0 are phenomenological dimensionless coefficients. The ansatz (2.8) is motivated from the entropy flux of 14 moments theory (Pavić *et al.* 2013), in which $\alpha_0 = \beta_0 = 2/(5 + \delta)$.

The internal degrees of freedom of such polyatomic matter have been addressed in literature as additional energy variables, see for example, (Pavić *et al.* 2013). Literature regarding such approaches appeared as early as 1967 (Kogan 1967) and has been used effectively thereafter in macroscopic modeling of polyatomic gases (Liu & Müller 1983; Pavić-Čolić 2014; Takashi Arima & Sugiyama 2018), producing the correct caloric equation of state for polyatomic gases. Of course the exact values for the phenomenological coefficients (α_0 , β_0) appearing in (2.9) depend on intricate nature of energy transfer mechanism among internal and translational degrees of freedom. Nevertheless, these can also be obtained through asymptotic reduction of the kinetic equation, which we shall briefly discuss after establishing the second-law inequality.

Substitution of the extended entropy flux Ψ from the last equation in (2.5), and balancing the terms give an extended second law

$$\frac{\partial(\rho\eta)}{\partial t} + \underline{\nabla} \cdot \left[\rho\eta \underline{\mathbf{v}} + \frac{\mathbf{q}}{\theta} - \frac{\alpha_0}{p\theta} \sigma \cdot \mathbf{q} - \frac{\beta_0}{p\theta} \Pi \mathbf{q} \right] = \Sigma, \quad (2.9)$$

where the entropy production term now reads

$$\begin{aligned} \Sigma = -\frac{\sigma}{\theta} : \left\langle \underline{\nabla \mathbf{v}} + \frac{\alpha_0}{p} \left\{ \underline{\nabla \mathbf{q}} - \frac{\mathbf{q} \underline{\nabla}(p\theta)}{2p\theta} \right\} \right\rangle - \frac{\Pi}{\theta} \left[\underline{\nabla \cdot \mathbf{v}} + \frac{\beta_0}{p} \left\{ \underline{\nabla \cdot \mathbf{q}} - \frac{\mathbf{q} \cdot \underline{\nabla}(p\theta)}{2p\theta} \right\} \right] \\ - \frac{\mathbf{q}}{\theta^2} \cdot \left[\underline{\nabla \theta} + \frac{\alpha_0}{\rho} \left\{ \underline{\nabla \cdot \sigma} - \frac{\sigma \cdot \underline{\nabla}(p\theta)}{2p\theta} \right\} + \frac{\beta_0}{\rho} \left\{ \underline{\nabla \Pi} - \frac{\Pi \underline{\nabla}(p\theta)}{2p\theta} \right\} \right]. \end{aligned}$$

Again, the entropy production forms a bilinear form as a sum of products of the thermodynamic fluxes and generalized thermodynamic forces. Once again, in order to guarantee the positivity of the entropy production, a linear flux-force relationship is assumed, which leads to the following coupled constitutive relations

$$\sigma = -2\mu \left\langle \underline{\nabla \mathbf{v}} + \frac{\alpha_0}{p} \left\{ \underline{\nabla \mathbf{q}} - \frac{\mathbf{q} \underline{\nabla}(p\theta)}{2p\theta} \right\} \right\rangle, \Pi = -\mu_b \left[\underline{\nabla \cdot \mathbf{v}} + \frac{\beta_0}{p} \left\{ \underline{\nabla \cdot \mathbf{q}} - \frac{\mathbf{q} \cdot \underline{\nabla}(p\theta)}{2p\theta} \right\} \right] \quad (2.10)$$

and

$$\mathbf{q} = -\kappa \left[\frac{\nabla\theta}{\rho} + \frac{\alpha_0}{\rho} \left\{ \nabla \cdot \boldsymbol{\sigma} - \frac{\boldsymbol{\sigma} \cdot \nabla(p\theta)}{2p\theta} \right\} + \frac{\beta_0}{\rho} \left\{ \nabla\Pi - \Pi \frac{\nabla(p\theta)}{2p\theta} \right\} \right]. \quad (2.11)$$

The stress (2.10) given by the CCR theory entails the hydrodynamic stress (underlined term) and the non-Newtonian second order corrections. Similarly, the heat flux equation (2.11) contains Fourier's law (underlined term), along with the second-order corrections to the heat flux.

In order to study non-equilibrium effects in rarefied polyatomic gases, Rahimi & Struchtrup (2014) introduced a set of 36 moment equations and further utilized the order of magnitude method to identify the leading order terms of all the moments appearing in the 36 moment theory. In their work the balance equations for the dynamic temperature $\vartheta = \Pi/\rho$ reads (eq. 35d in (Rahimi & Struchtrup 2014))

$$\rho \frac{D\vartheta}{Dt} + \frac{\delta}{3} \frac{2}{3+\delta} (\Pi \nabla \cdot \mathbf{v} + \boldsymbol{\sigma} : \nabla \mathbf{v}) + \frac{\delta}{3} \frac{2}{5+\delta} \nabla \cdot \boldsymbol{\Gamma} + \frac{\delta}{3} \frac{2}{3+\delta} \left(p \nabla \cdot \mathbf{v} + \frac{2}{5+\delta} \nabla \cdot \mathbf{q} \right) = -\frac{1}{\tau_{int}} \Pi \quad (2.12)$$

where D/Dt denotes the material time derivative, τ_{int} is the relaxation time for the dynamic temperature, and one defines $\boldsymbol{\Gamma} = \mathbf{q}^{tr} - \frac{5}{\delta} \mathbf{q}^{in}$; \mathbf{q}^{tr} and \mathbf{q}^{in} being the translational and the internal heat fluxes, respectively. Furthermore, using the Chapman-Enskog expansion (in τ_{in}), it is shown in the same article, that the underlined terms in last equation are higher order compared to the others, which can be assumed small in first order approximations. Neglecting these higher order terms, one gets the leading order constitutive relation for Π , as

$$\Pi^{(1)} = -\tau_{int} \frac{\delta}{3} \frac{2}{3+\delta} \left(p \nabla \cdot \mathbf{v} + \frac{2}{5+\delta} \nabla \cdot \mathbf{q} \right). \quad (2.13)$$

Comparing last equation with (2.10₂), one immediately recognizes

$$\tau_{int} = \frac{3}{\delta} \frac{3+\delta}{2} \frac{\mu_b}{p} \quad \text{and} \quad \beta_0 = \frac{2}{5+\delta}.$$

Similarly, the Chapman-Enskog expansion—via introducing a smallness parameter ε , and assuming $\varepsilon \sim O(\varepsilon^{1/2})$, $\tau_{tr} \sim O(\varepsilon^{\alpha/2})$, $\tau_{in} \sim O(\varepsilon^{1/2})$ and $0 < \alpha < 1$ —of the balance equation for heat flux follows (from eq. 35f in (Rahimi & Struchtrup 2014)), one again finds $\beta_0 = \frac{2}{5+\delta}$. Similar, arguments based upon the Chapman-Enskog can be made to justify $\alpha_0 = \frac{2}{5+\delta}$. Nevertheless, here we shall point out that the value for these phenomenological coefficients may vary with different collision models; consideration of which are beyond the scope of this article and throughout this article we shall assume

$$\alpha_0 = \frac{2}{5+\delta}, \quad \beta_0 = \frac{2}{5+\delta}. \quad (2.14)$$

Henceforth, we shall refer to (2.10–2.11) as polyatomic-CCR model.

3. Linearized and dimensionless equations

In this section, the equations, which we consider are dimensionless and linearized by introducing small perturbations from their values in a reference rest state defined by a constant pressure p_0 and a constant temperature θ_0 . The relations between the field variables and their dimensionless deviations (denoted with hat symbols) from their reference rest state are given as

$$p = p_0 (1 + \hat{p}), \quad \theta = \theta_0 (1 + \hat{\theta}), \quad \mathbf{v} = \sqrt{\theta_0} \hat{\mathbf{v}}, \quad \boldsymbol{\sigma} = p_0 \hat{\boldsymbol{\sigma}}, \quad \Pi = p_0 \hat{\Pi}, \quad \mathbf{q} = p_0 \sqrt{\theta_0} \hat{\mathbf{q}}, \quad \text{and} \quad \mathbf{x} = L \hat{\mathbf{x}},$$

where L is a characteristic length scale. The linearized and stationary ($\partial/\partial t \equiv 0$) conservation laws are given by

$$\nabla \cdot \hat{\mathbf{v}} = 0, \quad \nabla \cdot \left[(\hat{p} + \hat{\Pi}) \mathbf{I} + \hat{\boldsymbol{\sigma}} \right] = 0 \quad \text{and} \quad \nabla \cdot \hat{\mathbf{q}} = 0, \quad (3.1)$$

and the linearized stress, dynamic pressure and heat flux are specified as

$$\hat{\boldsymbol{\sigma}} = -2\text{Kn} \left\langle \nabla \hat{\mathbf{v}} + \frac{2}{\delta + 5} \nabla \hat{\mathbf{q}} \right\rangle, \quad \hat{\Pi} = 0 \quad \text{and} \quad \hat{\mathbf{q}} = -\frac{\text{Kn}c_p}{\text{Pr}} \left[\nabla \hat{\theta} + \frac{2}{\delta + 5} \nabla \cdot \hat{\boldsymbol{\sigma}} \right]. \quad (3.2)$$

In (3.2), the Knudsen number appears as the scaled viscosity $\text{Kn} = \mu_0 \sqrt{\theta_0} / (p_0 L)$, and $\text{Pr} = c_p \mu_0 / \kappa$ is the Prandtl number. Here, it is assumed that all the field variables are measured relative to their equilibrium values at infinity, hence all perturbations must vanish as $|\hat{\mathbf{x}}| \rightarrow \infty$.

3.1. Mathematical similarities between the CCR and NSF equations

It is worth noting that the steady, linearized CCR equations (3.1–3.2) can be converted to the Stokes-Fourier like system by introducing the following auxiliary variables,

$$\hat{\mathbf{V}} := \hat{\mathbf{v}} + \frac{2}{\delta + 5} \nabla \hat{\mathbf{q}} \quad \text{and} \quad \hat{\Theta} := \hat{\theta} - \frac{2}{\delta + 5} \hat{p}. \quad (3.3)$$

As a result, the linearized conservation laws (3.1) and (3.2) turn into

$$\nabla \cdot \hat{\mathbf{V}} = 0, \quad \nabla \hat{p} = \text{Kn} \Delta \hat{\mathbf{V}} \quad \text{and} \quad \Delta \hat{\Theta} = 0, \quad (3.4)$$

which are mathematically the same as the Stokes equations in $\{\hat{\mathbf{V}}, \hat{p}\}$ and the Laplace equation in $\hat{\Theta}$; however, now the Stokes equations are coupled with the Laplace equation via auxiliary variables $\hat{\mathbf{V}}$ and $\hat{\Theta}$. Nevertheless, from a mathematical point of view, the classical analytic solutions and techniques from potential theory (Batchelor 2000) for the Stokes and Laplace equations can be carried over to the slow, steady-state polyatomic-CCR model, as we show in next section.

In order to assess the accuracy of newly derived CCR model, we shall apply these equations to two classical boundary value problems (i) slow rarefied gas flow over a spherical particle, for which a closed form solution can be obtained, and (ii) slow rarefied gas flow over a doublet, which is solved numerically using the method of fundamental solution (MFS) (Lockerby & Collyer 2016; Rana *et al.* 2021*b*).

4. Slow rarefied gas flow over a spherical particle

First, we consider the case of a slow rarefied gas flow around a spherical particle of radius L . For this problem, solutions of the NSF equations are available (Batchelor 2000), giving the pressure \hat{p} , the velocity in radial direction \hat{u}_r and the azimuthal directions \hat{u}_ϕ as

$$\hat{p} = \text{Kn} \frac{a_1}{\hat{r}^2} \cos \phi, \quad \hat{u}_r = \hat{U}_\infty \left[1 + \frac{a_1}{\hat{r}} + \frac{a_2}{\hat{r}^3} \right] \cos \phi \quad \text{and} \quad \hat{u}_\phi = -\hat{U}_\infty \left[1 + \frac{a_1}{2\hat{r}} - \frac{a_2}{2\hat{r}^3} \right] \sin \phi, \quad (4.1)$$

in the spherical coordinate system. Here, $\hat{U}_\infty (= U_\infty / \sqrt{\theta_0})$ is the far-field velocity of the gas and $\hat{r} (= r/L)$ is the dimensionless radial distance, \hat{r} . The temperature and the heat flux are obtained as

$$\hat{\theta} = \frac{c_1}{\hat{r}^2} \cos \phi, \quad \hat{q}_r = \frac{2c_p \text{Kn}}{\text{Pr}} \frac{c_1 - \alpha_0 a_1 \text{Kn}}{\hat{r}^3} \cos \phi \quad \text{and} \quad \hat{q}_\phi = \frac{c_p \text{Kn}}{\text{Pr}} \frac{c_1 - \alpha_0 a_1 \text{Kn}}{\hat{r}^3} \sin \phi \quad (4.2)$$

The integration constants (a_1 , a_2 and c_1) are obtained by applying appropriate boundary conditions. The Stokes formula for the drag force exerted on a spherical particle due to the gas flow reads $\hat{F}_S = -6\pi \text{Kn} \hat{U}_\infty$, which is obtained by applying the classical no-slip and no-jump boundary condition at $\hat{r} = 1$, i.e., $\hat{u}_r = \hat{u}_\phi = 0$ and $\hat{\theta} = 0$ to the NSF solutions, i.e., equations

(4.1–4.2) with $\alpha_0 = 0$. The Stokes' drag formula is valid for $\text{Kn} \rightarrow 0$. Likewise, the NSF solutions with the standard first-order slip and temperature jump boundary conditions, i.e.,

$$\hat{u}_r = 0, \hat{u}_\phi = -\sqrt{\frac{\pi}{2}}\hat{\sigma}_{r\phi} \quad \text{and} \quad \hat{\theta} = -\frac{2}{(4+\delta)}\sqrt{\frac{\pi}{2}}\hat{q}_r, \quad (4.3)$$

yield drag force $\hat{F}_D = \hat{F}_S \left(2\text{Kn} + \sqrt{2/\pi} \right) / \left(3\text{Kn} + \sqrt{2/\pi} \right)$. In (4.3), the accommodation coefficients are taken to be unity (Sharipov 2011).

The second order boundary conditions which shall be used for the polyatomic-CCR solutions (4.1–4.2), read

$$\hat{u}_r = 0, \hat{u}_\phi = -\sqrt{\frac{\pi}{2}}\hat{\sigma}_{r\phi} - \frac{3}{4}\hat{q}_\phi \quad \text{and} \quad \hat{\theta} = -\frac{2}{(4+\delta)}\sqrt{\frac{\pi}{2}}\hat{q}_r - \frac{3}{4}\hat{\sigma}_{rr}. \quad (4.4)$$

Here, the first boundary condition (4.4.1) represents the non-penetration condition on a solid wall. The slip boundary condition (4.4.2) defines the velocity slip at the wall, which relates the tangential gas velocity slip the tangential shear stress and heat flux. The slip boundary condition, when compared to the second-order boundary conditions from the literature (Deissler 1964; Lockerby *et al.* 2004; Zhang *et al.* 2012) gives the first-order and second-order slip coefficients as $A_1 = 1$ and $A_2 = \frac{3}{2\pi} \frac{1}{\text{Pr}} = 0.682$; see Appendix A for details. The third boundary condition (4.4.3) is the temperature-jump boundary condition, where the temperature jump coefficient $\zeta_T = \frac{\sqrt{\pi}}{2} \frac{2}{4+\delta} \frac{c_p}{\text{Pr}}$ (Sharipov 2011) and the accommodation coefficient being one. An additional term in (4.4.3) appears as a consequence of the Onsager symmetry (Rana *et al.* 2018, 2021a).

It should be noted here that values for the slip and jump coefficients vary in literature (Sharipov 2011) and one may perform asymptotic expansions—taking into account the so-called Knudsen layer corrections (Rana & Struchtrup 2016)—to fit theory/experimental results. Indeed, in (4.4.2) the coefficient $3/4$ (which is equivalent of taking an appropriate value for the second-order slip coefficient A_2) was chosen so that it gives good fit for the drag coefficient for a sphere; see Appendix A for further details along with the sensitivity analysis of the results on slip/jump coefficients. In particular, the considered choice of A_2 significantly overestimate the value for thermal slip coefficient (Sharipov 2011). Nevertheless, for the problems considered in this paper, the effects of thermal slip coefficient are negligible.

Substitution of the CCR solutions (4.1–4.2) in (4.4) gives integration constants (a_1, a_2 and c_1), which in turn provide a closed form expression for the drag as

$$\hat{F}_D = \hat{F}_S \left(1 + kn \frac{1 + \left(\frac{3kn}{2\pi} \frac{1+4\frac{3\delta+19}{\delta+5}kn}{\text{Pr}+2\frac{\delta+3}{\delta+4}kn} \right)}{1 + kn \left(2 + \frac{9kn}{4\pi} \frac{3-\delta}{\text{Pr}+2\frac{\delta+5}{\delta+4}kn} \right)} \right)^{-1} \quad (4.5)$$

where, for brevity, we have introduced a modified Knudsen number $kn = \sqrt{\frac{\pi}{2}}\text{Kn}$. Clearly, $\hat{F}_D \rightarrow \hat{F}_S$ as $\text{Kn} \rightarrow 0$ and $\hat{F}_D/\hat{F}_S \rightarrow 0$ as $\text{Kn} \rightarrow \infty$, hence the continuum and the free-molecular regimes are recovered, qualitatively.

In Fig. (1a) the drag force \hat{F}_D normalized with Stokes' drag \hat{F}_S is shown as a function of the Knudsen number. The results obtained from the polyatomic-CCR model (solid blue), first-order NSF (dashed red) and Stokes' formula (thin green) are compared with the experimental results (black dot-dashed lines and symbols) given by Allen & Raabe (1982).

For larger values of the Knudsen number, the force decreases. Notably, for the NSF with the first-order boundary conditions the drag force reaches a finite value ($2/3$) as $\text{Kn} \rightarrow \infty$, which contradicts experimental observations. The polyatomic-CCR results match with the experiment quite remarkably even for large value of the Knudsen number. In the above computations, transport

properties are taken to be for dry air, i.e., $\text{Pr} = 0.7$ and $\delta = 2$, which gives the ratio of the specific heats $\gamma = 1.4$ —a value consistent with air/nitrogen at moderate temperatures.

5. Slow rarefied gas flow over a doublet

In this section we shall consider the non-trivial case of flow over a doublet for which we shall apply the method of fundamental solution (MFS) technique. However, before that, we first formulate the Green functions associated with the polyatomic-CCR model (3.1–3.2).

5.1. Green's functions and the method of fundamental solutions

Green's functions for the Stokes equations and the Laplace equations are obtained as a response of the fluid with regard to a point body force $\hat{\mathbf{f}}$ in the momentum equation (Stokeslet) and a heat source of strength \hat{g} (Thermlet) in the energy balance equation (Lockerby & Collyer 2016; Rana *et al.* 2021b). Green's functions associated with the polyatomic-CCR equations follow from the Stokeslet and Thermlet, as

$$\hat{\mathbf{v}}(\hat{\mathbf{r}}) = \frac{1}{8\pi} \left(\frac{\hat{\mathbf{r}}\hat{\mathbf{r}}}{|\hat{\mathbf{r}}|^3} + \frac{\mathbf{I}}{|\hat{\mathbf{r}}|} \right) \cdot \hat{\mathbf{f}} + \frac{3\alpha_0^2 c_p \text{Kn}^2}{4\pi \text{Pr} |\hat{\mathbf{r}}|^5} \langle \hat{\mathbf{r}}\hat{\mathbf{r}} \rangle \cdot \hat{\mathbf{f}}, \quad (5.1a)$$

$$\hat{p}(\hat{\mathbf{r}}) = \frac{\text{Kn} \hat{\mathbf{f}} \cdot \hat{\mathbf{r}}}{4\pi |\hat{\mathbf{r}}|^3} \quad \text{and} \quad \hat{\sigma}(\hat{\mathbf{r}}) = \frac{3\text{Kn}}{4\pi |\hat{\mathbf{r}}|^5} \left(\hat{\mathbf{f}} \cdot \hat{\mathbf{r}} + \underline{2\alpha_0 \text{Kn} \hat{g}} \right) \langle \hat{\mathbf{r}}\hat{\mathbf{r}} \rangle, \quad (5.1b)$$

where $\hat{\mathbf{r}} = \hat{\mathbf{x}} - \hat{\mathbf{x}}^s$ is the position of an arbitrary point $\hat{\mathbf{x}}$ from the computational domain relative to the singularity point located at $\hat{\mathbf{x}}^s$ (a point outside of the computational domain).

The temperature \hat{T} and heat flux $\hat{\mathbf{q}}$ are obtained as

$$\hat{T}(\hat{\mathbf{r}}) = \frac{\text{Pr}}{4\pi c_p} \frac{\hat{g}}{|\hat{\mathbf{r}}|} \quad \text{and} \quad \hat{\mathbf{q}}(\hat{\mathbf{r}}) = \frac{\text{Kn}}{4\pi} \frac{\hat{g}}{|\hat{\mathbf{r}}|^3} \hat{\mathbf{r}} - \frac{3\alpha_0 c_p \text{Kn}^2}{4\pi \text{Pr} |\hat{\mathbf{r}}|^5} \langle \hat{\mathbf{r}}\hat{\mathbf{r}} \rangle \cdot \hat{\mathbf{f}}. \quad (5.2)$$

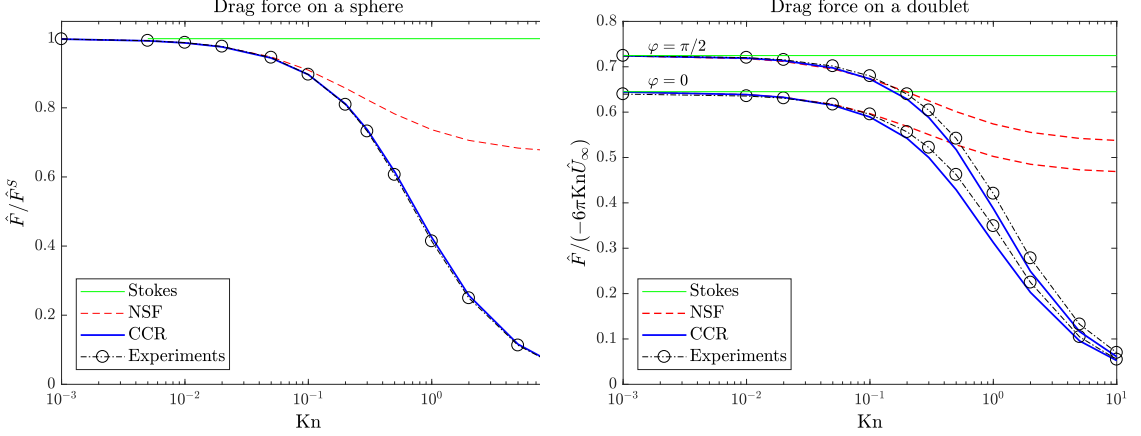
In the polyatomic-CCR Green's functions (5.1–5.2), the coupling between the Stokeslet and Thermlet occurs due to the underlined term. Obviously, for the classic NSF equations ($\alpha_0 = 0$), such coupling is absent and one obtains classical Stokeslet and Thermlet.

5.2. Drag on a doublet

In Fig. (1b), we show the drag force on a doublet using the MFS technique developed by Lockerby & Collyer (2016); Rana *et al.* (2021b) for the case of monoatomic gases. The essential idea behind MFS is to decompose the solutions of the linearized partial differential equations as superposition of the Green's functions, where the weights are determined such that the boundary conditions are satisfied at some boundary nodes (collocation points).

In particular, we study a doublet moving with an angle of φ between the flow direction and the line joining the centers of the doublet. This is an interesting case to be considered because (i) it is a full 3D problem and no closed form analytic solution exists (ii) experimental results are available for this problem in the literature (Cheng *et al.* 1988) for $\varphi = 0$ and $\varphi = \pi/2$ (Cheng *et al.* 1988). The overall agreement of the polyatomic-CCR model's drag force with the experimental data is excellent in both the cases ($\varphi = 0, \pi/2$) and as before, the NSF theory over-predicts the drag.

So far, we have considered steady-state slow rarefied flow conditions for which the polyatomic-CCR model can be transformed into the NSF-like equations and analytic/semi-analytic approaches can be utilized. For the considered cases, the dynamic temperature identically vanishes and the polyatomic nature of the gas only appear through Pr , μ , c_p , c_v , α_0 and β_0 , where last two values being $2/5$ and 0 for monoatomic gases, respectively. For non-linear (for example, shocks in hyper-sonic flows) or transient process (for example, wave propagation and Rayleigh-Brillouin scattering in polyatomic gases), other polyatomic effects might manifest itself.



(a) The normalised drag force (with Stokes' drag) on a sphere against Knudsen number. The results computed from the NSF with first-order slip and the polyatomic-CCR model to its line of centres ($\varphi = 0$) and flow perpendicular to its axis ($\varphi = \pi/2$) are compared with the experimental data by Allen & Raabeline of centres (Allen & Raabeline (1982)). The experimental data are taken from Cheng *et al.* (1988).

Figure 1

6. Normal shock structure in nitrogen

Finally, in order to assess the effects of non-linear terms, we shall now use the polyatomic-CCR model to compute the shock structure in nitrogen gas. The normal shock structure problem is modelled as a one-dimensional problem so that the field variables (velocity, stress tensor and heat flux vector, etc.) have only non-zero x -component. In the frame of reference of the moving shock (in the x -direction), the gas upstream and downstream is assumed to be in equilibrium state with $(\rho, v_x, \theta) = (\rho_0, U_0, \theta_0)$ and $(\rho, v_x, \theta) = (\rho_\infty, v_\infty, \theta_\infty)$, respectively. The upstream and downstream conditions are linked to each other by the Rankine-Hugoniot relations (Anderson 2003):

$$\frac{\rho_\infty}{\rho_0} = \frac{(\gamma + 1)Ma^2}{2 + Ma^2(\gamma - 1)}, \quad \frac{\rho_\infty v_\infty}{\rho_0 \sqrt{\theta_0}} = \sqrt{\gamma}Ma, \quad \text{and} \quad \frac{\rho_\infty \theta_\infty}{\rho_0 \theta_0} = \frac{1 - \gamma + 2\gamma Ma^2}{1 + \gamma} \quad (6.1)$$

where $Ma = U_0/\sqrt{\gamma\theta_0}$ is the Mach number defined in terms of the upstream condition.

The mean free path based upon the upstream conditions can be defined as $\lambda_0 = (8\sqrt{2}\mu_0)/(5\rho_0\sqrt{\pi\theta_0})$, where μ_0 is the viscosity in the upstream state. For the shock problem, the polyatomic-CCR model reduces to

$$\tau_{xx} := \Pi + \sigma_{xx} = -\frac{4\mu}{3} \left(1 + \frac{\delta}{2(3+\delta)}Z \right) \left(\frac{dv_x}{dx} + \frac{\alpha_0}{p} \left\{ \frac{dq_x}{dx} - \frac{q_x}{2p\theta} \frac{d(p\theta)}{dx} \right\} \right), \quad (6.2)$$

$$q_x = -\frac{\mu c_p}{Pr} \left[\frac{d\theta}{dx} + \frac{\alpha_0}{\rho} \left\{ \frac{d(\Pi + \sigma_{xx})}{dx} - \frac{\Pi + \sigma_{xx}}{2p\theta} \frac{d(p\theta)}{dx} \right\} \right]. \quad (6.3)$$

Here, for convenience, we have defined $\tau_{xx} = \Pi + \sigma_{xx}$ and introduced Z as the dimensionless rotational collision number. The viscosity is obtained from the Sutherland's law and Z from Parker's formula (Parker 1959) as

$$\mu = \mu_0 \left(\frac{T}{T_0} \right)^{3/2} \frac{T_0 + T_S}{T + T_S}, \quad \text{and} \quad Z := \frac{3(3+\delta)\mu_b}{2\delta\mu} = \frac{Z_\infty}{1 + \frac{\pi^{3/2}}{2} \sqrt{\frac{T^*}{T}} + \left(\frac{\pi^2}{4} + \pi \right) \frac{T^*}{T}} \quad (6.4)$$

where $T_S = 107\text{K}$ is the Sutherland's constant, $Z_\infty = 18.2$ and $T^* = 91.5\text{K}$. The reduced system of

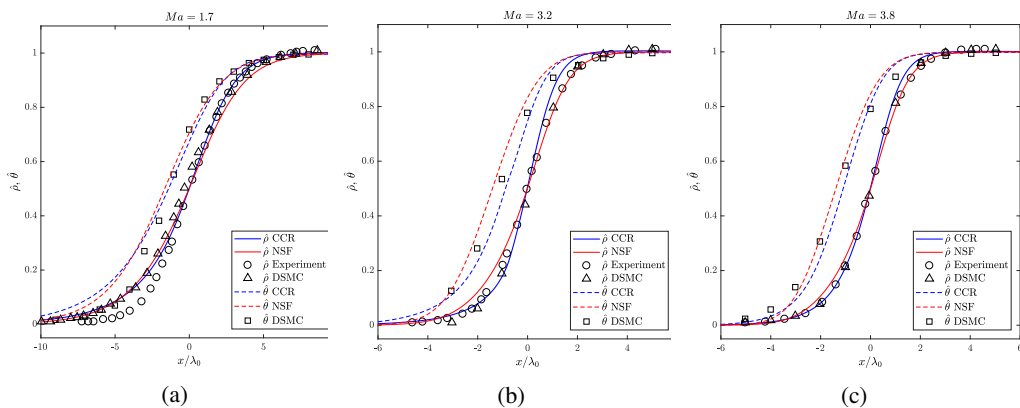


Figure 2: Comparison of reduced density and temperature profiles obtained using the polyatomic-CCR models with the experimental measurements of Alsmeyer (1976) for Mach numbers: (a) $Ma = 1.7$ (b) $Ma = 3.2$ and (c) $Ma = 3.8$.

ordinary differential equations are numerically solved using a second order central finite difference scheme with boundary conditions (6.1).

Figure (2) shows the profiles of reduced density, $\hat{\rho} := (\rho - \rho_0)/(\rho_\infty - \rho_0)$ and reduced temperature, $\hat{\theta} := (\theta - \theta_0)/(\theta_\infty - \theta_0)$ vs x/λ_0 for three Mach numbers, $Ma = 1.7$ (2.a), $Ma = 3.2$ (2.b) and $Ma = 3.8$ (2.c). For a smaller Mach number ($Ma = 1.7$), the macroscopic theories and the DSMC give a good agreement. At higher Mach numbers (2.b, c), the upstream region of the shock is resolved accurately by the polyatomic-CCR model whereas some deviations are observed in the downstream region. Interestingly, for the NSF theory we observe an opposite behaviour. For the temperature shock profiles, the DSMC predictions appear to be slight narrower than the macroscopic theories. The NSF theory slightly over-predicts the temperature while the polyatomic-CCR theory under-predicts it. The main goal of the present study was to derive the polyatomic-CCR model and demonstrate its usefulness for some practical applications; a thorough test of these equations for the shock wave flow problems is beyond the scope of this article. Nevertheless, for the considered range of the Mach number, the overall results from the polyatomic-CCR model are in good agreement with the experimental data.

This is noteworthy given that the entropy current density we assume has been derived in (Pavić *et al.* 2013). It employs the exponential distribution function in kinetic theory and the entropy of this distribution is analytically obtained by integrating over internal degrees of freedom and particular velocity. This procedure crucially depends on the concept of local temperature which has been used in the exponential distribution. Despite the difficulties in this concept, it turns out that local temperature may thus be fruitfully applied to rarefied flows of poly-atomic gases as well.

7. Conclusion and future directions

CIT framework applied to rarefied flows require justification for the local equilibrium hypothesis which is taken to hold in the case of rarefied gases. There have been several objections to that assumption, especially regarding the concept of local temperature and entropy. However, under the RET assumption of entropy current density subject to a different constitutive law, CCR modelling of rarefied gas flows extends the applicability beyond classical NSF equation whilst maintaining the same mathematical and thermodynamical structure. Good agreement of CCR has been previously obtained with experiments in the case of monoatomic gases. In this article, we have

proposed a polyatomic-CCR model, and obtained its solutions for some classical flow problems, namely slow flow past an aerosol of different shapes. Further these have been benchmarked with experimental data from the literature. The polyatomic-CCR theory provides an excellent match with experimental observations over the range of all Knudsen numbers. We have also computed the normal shock structure using the polyatomic-CCR model. A very good agreement was observed with the kinetic theory, as well as with the experimental data.

We have formulated Green's functions and a MFS technique for the polyatomic-CCR model, which in principle, allow for simulations of slow polyatomic gas flow over any arbitrary shapes and sizes. Thus, from a modelling perspective, a simultaneously computationally efficient and accurate (to nano-scales) method has been proposed. For a future direction, a machine learning algorithm trained using the data from the polyatomic-CCR framework is planned, which can provide simulation-for-design tool to study the multi-scale process of dispersion and dynamics of UFPs in air.

The proposed model is found to possess three important limitations which could be worked upon in the future. They involve thermodynamic issues related to local equilibrium, temperature dependent specific heats and asymptotic consistency of higher order boundary conditions. For example, the last issue assumes importance when one deals with flows with thermal transpiration (eg., Knudsen pump). We comment upon these below. The proposed model assumes the validity of local equilibrium. This assumption cannot be justified when the bulk-to-shear-viscosity ratio is very large; for example, the carbon dioxide gas has the bulk-to-shear-viscosity ratio ~ 2000 . Conceptually, in addition, the definition of local thermodynamic quantities has been questioned. Temperature and entropy have been emphasized the most in this regard. The proportionality of internal energy and temperature has been especially a crucial assumption which requires to be addressed. In a scenario like this, an interesting approach could be to use an extended Gibbs' equation in order to get a refined NSF equations or the corresponding coupled constitutive relations (Ruggeri 2015).

The polyatomic-CCR theory developed here assumes the constant specific heats (hence δ to be constant). In hindsight of the results in the Section 6, it is worthwhile to discuss the validity of this assumption. For the range of Mach number considered in this article ($1.7 \leq \text{Ma} \leq 4$) the maximum temperature variations—from (6.1)—are $1.46 \leq \frac{\theta_\infty}{\theta_0} \leq 4.0s$, which are seemingly high. However, for the nitrogen gas, the change in δ between 200K–800K is about $\lesssim 7.5\%$ (Borgnakke & Sonntag 2009), therefore the assumption of δ being constant was justifiable. Nevertheless, for large enough temperature variations, this assumption may not hold true and an extension of the CCR model for temperature dependent specific heats (i.e., assuming $\delta = \delta(\theta)$) will be sought.

Furthermore, the boundary conditions (4.4) employed in Section 4-5 were obtained in a way to fit the drag coefficient on the sphere (by choosing appropriate value of the second-order slip coefficient). The asymptotic analysis (see also, Appendix A) suggests that these boundary conditions may lead to erroneous predictions in situations when thermal transpiration/thermal-stress play important role. A detailed analysis of such flows along with a consistent set of boundary conditions for the polyatomic-CCR theory is also planned for the future.

8. Funding

This work has been financially supported by "SRG" project SRG/2021/000790 funded by the Science & Engineering Research Board, India.

9. Declaration of interests

The authors report no conflict of interest.

Appendix A. Asymptotic analysis of the boundary conditions

Here, we shall carry out a comparison of boundary conditions (4.4) with those from the literature and discuss qualitative effects of different terms appearing in the boundary conditions. The (linearized and dimensionless) generalized slip boundary condition relates the tangential gas velocity slip \hat{V}_i to the tangential shear stress and heat flux, as (Lockerby *et al.* 2004)

$$\begin{aligned} \hat{V}_i t_i = & A_1 \sqrt{\frac{\pi}{2}} \text{Kn} \left(\frac{\partial \hat{v}_i}{\partial \hat{x}_j} + \frac{\partial \hat{v}_j}{\partial \hat{x}_i} \right) n_i t_j - A_2 \left(\sqrt{\frac{\pi}{2}} \text{Kn} \right)^2 \frac{\partial}{\partial \hat{x}_k} \left(\frac{\partial \hat{v}_i}{\partial \hat{x}_k} + \frac{\partial \hat{v}_k}{\partial \hat{x}_i} \right) t_i \\ & + A_3 \text{Kn} \frac{\partial \hat{\theta}}{\partial \hat{x}_i} t_i - A_4 \sqrt{\frac{\pi}{2}} \text{Kn}^2 \frac{\partial^2 \hat{\theta}}{\partial \hat{x}_i \hat{x}_j} n_i t_j, \end{aligned} \quad (\text{A } 1)$$

where n_i is unit normal pointing from the boundary into the gas and t_i is a tangential direction. In the last equation, A_1 and A_2 are the first-order and second-order slip coefficients, respectively. Furthermore, A_3 is thermal slip coefficient (Sharipov 2011) †, which gives rise to thermal creep, and the last term (with A_4) is due to the thermal-stress slip flow (Lockerby *et al.* 2004). ‡

The boundary conditions (4.4), when written in the Cartesian coordinates, read

$$\hat{\sigma}_{ij} n_i t_j = -\sqrt{\frac{2}{\pi}} \frac{\chi}{2 - \chi} \frac{1}{\eta_{\text{VS}}} \left(\hat{V}_i + \eta^1 \hat{q}_i \right) t_i, \quad (\text{A } 2)$$

$$\hat{q}_k n_k = -\sqrt{\frac{2}{\pi}} \frac{\chi}{2 - \chi} \frac{4 + \delta}{2} \frac{1}{\eta_{\text{TJ}}} \left(\hat{T} + \eta^1 \hat{\sigma}_{ij} n_i n_j \right). \quad (\text{A } 3)$$

Here, we have further introduced the accommodation coefficient χ , the velocity-slip coefficient η_{VS} and the temperature-jump coefficient η_{TJ} . For the calculations performed in Section 4-5, we had taken $\chi = \eta_{\text{VS}} = \eta_{\text{TJ}} = 1$ and $\eta^1 = 3/4$; below we provide a rationale for this choice.

Substituting the CCR (3.2) into (A 2) and using the conservation laws (3.1), one gets

$$\begin{aligned} \hat{V}_i t_i = & \sqrt{\frac{\pi}{2}} \text{Kn} \frac{2 - \chi}{\chi} \eta_{\text{VS}} \left(\frac{\partial \hat{v}_i}{\partial \hat{x}_j} + \frac{\partial \hat{v}_j}{\partial \hat{x}_i} \right) n_i t_j + \eta^1 \frac{\text{Kn}}{\text{Pr}} \frac{\partial \hat{\sigma}_{ik}}{\partial \hat{x}_k} t_i \\ & + \frac{\eta^1 c_p}{\text{Pr}} \text{Kn} \frac{\partial \hat{\theta}}{\partial \hat{x}_i} t_i + \sqrt{\frac{\pi}{2}} \frac{2 - \chi}{\chi} \eta_{\text{VS}} \text{Kn} \frac{2}{5 + \delta} \left(\frac{\partial \hat{q}_i}{\partial \hat{x}_j} + \frac{\partial \hat{q}_j}{\partial \hat{x}_i} \right) n_i t_j. \end{aligned} \quad (\text{A } 4)$$

In order to compare the last equation with (A 1), $\hat{\sigma}_{ik}$ and \hat{q}_i need to be replaced by the corresponding NSF equations, i.e., by $\hat{\sigma}_{ik}^{\text{NSF}}$ and \hat{q}_i^{NSF} , to get

$$\begin{aligned} \hat{V}_i t_i = & \sqrt{\frac{\pi}{2}} \text{Kn} \frac{2 - \chi}{\chi} \eta_{\text{VS}} \left(\frac{\partial \hat{v}_i}{\partial \hat{x}_j} + \frac{\partial \hat{v}_j}{\partial \hat{x}_i} \right) n_i t_j - \eta^1 \frac{\text{Kn}^2}{\text{Pr}} \frac{\partial}{\partial \hat{x}_k} \left(\frac{\partial \hat{v}_i}{\partial \hat{x}_k} + \frac{\partial \hat{v}_k}{\partial \hat{x}_i} \right) t_i \\ & + \frac{\eta^1 c_p}{\text{Pr}} \text{Kn} \frac{\partial \hat{\theta}}{\partial \hat{x}_i} t_i + \sqrt{\frac{\pi}{2}} \text{Kn} \frac{2 - \chi}{\chi} \eta_{\text{VS}} \frac{2}{5 + \delta} \left(\frac{\partial \hat{q}_i^{\text{NSF}}}{\partial \hat{x}_j} + \frac{\partial \hat{q}_j^{\text{NSF}}}{\partial \hat{x}_i} \right) n_i t_j. \end{aligned} \quad (\text{A } 5)$$

Comparing the last equation with a generalized slip boundary condition (A 1), one identifies

$$A_1 = \frac{2 - \chi}{\chi} \eta_{\text{VS}}, \quad A_2 = \frac{2}{\pi} \frac{\eta^1}{\text{Pr}}, \quad \text{and} \quad A_3 = \frac{\eta^1 c_p}{\text{Pr}} = \sigma_T. \quad (\text{A } 6)$$

There exists a vast literature documenting values of the first-order and second-order slip coefficients (Zhang *et al.* 2012); few are tabulated in Table 1. As we can see from the table,

† In Sharipov's notation $A_3 = \sigma_T$.

‡ In Lockerby's notation the mean free path is defined as $\lambda = \sqrt{\pi/2} \text{Kn} L$, and in Sharipov's notation $A_1 = 2\sigma_P/\sqrt{\pi}$ where σ_P is defined as the viscous slip coefficient in Sharipov (2011) Table 1, and ℓ is defined by as $\ell = \sqrt{2} \text{Kn} L$.

	A_1	A_2	Model
Deissler (1964)	1	9/8	Monoatomic/polyatomic
Struchtrup & Torrilhon (2008)	1	0.531	Monoatomic/R13
Li <i>et al.</i> (2011)	1	0.8	Lattice Boltzmann
Gibelli (2012)	1.1144	0.4952	Monoatomic/hard-sphere Boltzmann
Lockerby <i>et al.</i> (2004)	1	0.145 – 0.19	Monoatomic/polyatomic
Hadjiconstantinou (2003)	1.11	0.61	Monoatomic/hard-sphere Boltzmann
Sharipov (2011)	1.1 – 1.14	–	BGK/hard-sphere Boltzmann
Present model	1	0.682	CCR theory

Table 1: Values of the first-order and second-order slip coefficients (Zhang *et al.* 2012).

the value for A_1 is around unity, however, no conclusion can be reached on the correct value of the coefficient A_2 ; the value for $A_2 (= \frac{3}{2\pi} \frac{1}{Pr})$ was chosen so that it gives good match for the drag coefficient for sphere. However, for the chosen values of A_2 , the presented boundary conditions yields $A_3 = \frac{3}{4} \frac{c_p}{Pr}$, which is about 3.5 times as then the reported values; in (Sharipov 2011), the value A_3 ranges between 0.94 – 1.12. Therefore, one would expect that the presented model/boundary conditions will not provide adequate results for problems involving thermal creep/thermal-stress. In order to tackle such problems, one might choose η^1 appropriately (instead of 3/4) to get the correct value for A_3 ; however, this is beyond the scope of this article.

Similarly, substituting the CCR (3.2) into (A 3) and using the conservation laws, one obtains

$$\hat{T} = \zeta_T \sqrt{2} Kn \frac{\partial \hat{\theta}}{\partial \hat{x}_k} n_k + \sqrt{\frac{\pi}{2}} \frac{2 - \chi}{\chi} \frac{2\eta_{TJ}}{4 + \delta} \frac{Kn}{Pr} \frac{\partial \hat{\sigma}_{kr}}{\partial \hat{x}_r} n_k - \eta^1 \hat{\sigma}_{ij} n_i n_j, \quad (\text{A } 7)$$

where

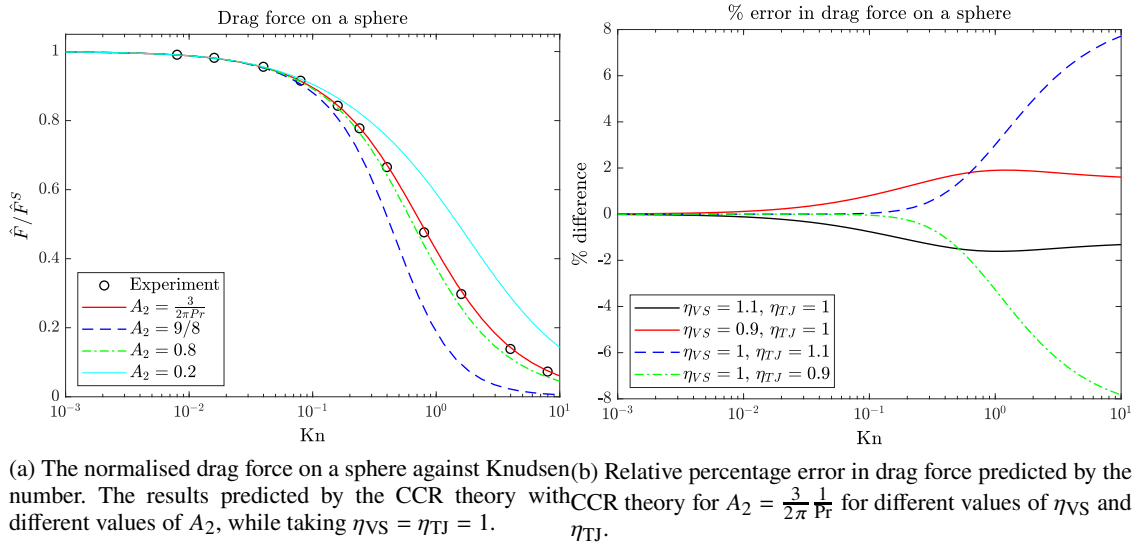
$$\zeta_T = \frac{\sqrt{\pi}}{2} \frac{2 - \chi}{\chi} \frac{2\eta_{TJ}}{4 + \delta} \frac{c_p}{Pr}. \quad (\text{A } 8)$$

Here, ζ_T is the temperature jump coefficient (Sharipov 2011). The reported value for ζ_T by Sharipov (2011) is $\zeta_T = \frac{\sqrt{\pi}}{2} \frac{2}{4 + \delta} \frac{c_p}{Pr} \left(\frac{2 - \chi}{\chi} + 0.17 \right)$; which is about 17% higher than considered value.

In order to quantify the change in drag coefficient with respect to the slight variations in A_2 (the second-order slip coefficient), η_{VS} , η_{TJ} , in Fig. (3a) we plot the drag on a sphere with different values of A_2 , while taking $\eta_{VS} = \eta_{TJ} = 1$. The second-order slip coefficient has a notable effect on the drag, in particular at large values for the Knudsen number. On the other hand, the small variations in values for η_{VS} η_{TJ} lead to slight change in drag coefficients—as seen in Fig. (3b)—which is less than 10% within the reported values of η_{VS} and η_{TJ} .

REFERENCES

- ALLEN, M. & RAABE, O. 1982 Re-evaluation of Millikan's oil drop data for the motion of small particles in air. *J. Aerosol Sci* **13** (6), 537–547.
- ALSMeyer, H. 1976 Density profiles in argon and nitrogen shock waves measured by the absorption of an electron beam. *J. Fluid Mech.* **74** (3), 497–513.
- ANDERSON, J. 2003 *Modern Compressible Flow: With Historical Perspective*. Aeronautical and Aerospace Engineering Series . McGraw-Hill Education.
- BATCHELOR, G. 2000 *An introduction to fluid dynamics*. Cambridge University Press.
- BORGNACKE, C. & SONNTAG, R. E. 2009 *Fundamentals of thermodynamics: Part 1*. John Wiley & Sons, Inc.
- CAI, Z. & LI, R. 2014 The NRXX method for polyatomic gases. *J. Comput. Phys.* **267**, 63–91.
- CHAPMAN, S. & COWLING, T. G. 1970 *The Mathematical Theory of Non-Uniform Gases*. Cambridge: Cambridge University Press.



(a) The normalised drag force on a sphere against Knudsen number. The results predicted by the CCR theory with different values of A_2 , while taking $\eta_{VS} = \eta_{TJ} = 1$. (b) Relative percentage error in drag force predicted by the CCR theory for $A_2 = \frac{3}{2\pi Pr}$ for different values of η_{VS} and η_{TJ} .

Figure 3

- CHENG, Y.-S., ALLEN, M. D., GALLEGOS, D. P., YEH, H.-C. & PETERSON, K. 1988 Drag force and slip correction of aggregate aerosols. *Aerosol Science and Technology* **8** (3), 199–214.
- DE FALCO, G., COLARUSSO, C., TERLIZZI, M., POPOLO, A., PECORARO, M., COMMODO, M., MINUTOLO, P., SIRIGNANO, M., D'ANNA, A., AQUINO, R. P., PINTO, A., MOLINO, A. & SORRENTINO, R. 2017 Chronic obstructive pulmonary disease-derived circulating cells release IL-18 and IL-33 under ultrafine particulate matter exposure in a caspase-1/8-independent manner. *Frontiers in Immunology* **8**, 1415.
- DEISSLER, R. 1964 An analysis of second-order slip flow and temperature-jump boundary conditions for rarefied gases. *Int. J. Heat Mass Transf.* **7** (6), 681–694.
- GIBELLI, L. 2012 Velocity slip coefficients based on the hard-sphere Boltzmann equation. *Phys. Fluids* **24** (2), 022001.
- GRAD, H. 1958 Principles of the kinetic theory of gases. In *Thermodynamik der Gase, Handbuch der Physik*, vol. 3 / 12, pp. 205–294. Berlin: Springer.
- HADJICONSTANTINOIU, N. G. 2003 Comment on Cercignani's second-order slip coefficient. *Phys. Fluids* **15** (8), 2352–2354.
- JUNK, M. & UNTERREITER, A. 2002 Maximum entropy moment systems and galilean invariance. *Contin. Mech. Thermodyn.* **14** (6), 563–576.
- KOGAN, M. 1967 *On the principle of maximum entropy, in Rarefied Gas Dynamics*, , vol. I. Academic Press, New York.
- KREMER, G. M. 2010 *An Introduction to the Boltzmann Equation and Transport Processes in Gases*. Berlin: Springer.
- LI, Q., HE, Y. L. & TANG, G. H. 2011 Lattice Boltzmann modeling of microchannel flows in the transition flow regime. *Microfluid Nanofluid* **10**, 607–618.
- LIU, I.-S. & MÜLLER, I. 1983 Extended thermodynamics of classical and degenerate ideal gases. *Arch. Rational. Mech. Anal.* **83**, 285–332.
- LOCKERBY, D. A. & COLLYER, B. 2016 Fundamental solutions to moment equations for the simulation of microscale gas flows. *J. Fluid Mech.* **806**, 413–436.
- LOCKERBY, D. A., REESE, J. M., EMERSON, D. R. & BARBER, R. W. 2004 Velocity boundary condition at solid walls in rarefied gas calculations. *Phys. Rev. E* **70**, 017303.
- MALLINGER, F. 1998 Generalization of the Grad theory to polyatomic gases. Research Report RR-3581, INRIA.
- MÜLLER, I. & RUGGERI, T. 2013 *Rational extended thermodynamics*, , vol. 37. Springer Science & Business Media.
- PARKER, J. G. 1959 Rotational and vibrational relaxation in diatomic gases. *Phys. Fluids* **2** (4), 449–462.

- PAVIĆ, M., RUGGERI, T. & SIMIĆ, S. 2013 Maximum entropy principle for rarefied polyatomic gases. *Physica A: Statistical Mechanics and its Applications* **392** (6), 1302–1317.
- PAVIĆ-ČOLIĆ, M. SIMIĆ, S. 2014 Moment equations for polyatomic gases. *Acta Appl. Math.* **132**, 469–482.
- RAHIMI, B. & STRUCHTRUP, H. 2014 Capturing non-equilibrium phenomena in rarefied polyatomic gases: A high-order macroscopic model. *Phys. Fluids* **26**, 052001.
- RANA, A. S., GUPTA, V. K., SPRITTLES, J. E. & TORRILHON, M. 2021a *h*-theorem and boundary conditions for the linear R26 equations: application to flow past an evaporating droplet. *J. Fluid Mech.* **924**, A16.
- RANA, A. S., GUPTA, V. K. & STRUCHTRUP, H. 2018 Coupled constitutive relations: a second law based higher-order closure for hydrodynamics. *Proc. Roy. Soc. A* **474**, 20180323.
- RANA, A. S., SAINI, S., CHAKRABORTY, S., LOCKERBY, D. A. & SPRITTLES, J. E. 2021b Efficient simulation of non-classical liquid–vapour phase-transition flows: a method of fundamental solutions. *J. Fluid Mech.* **919**, A35.
- RANA, A. S. & STRUCHTRUP, H. 2016 Thermodynamically admissible boundary conditions for the regularized 13 moment equations. *Phys. Fluids* **28** (2), 027105.
- RUGGERI, T. 2015 Non-linear maximum entropy principle for a polyatomic gas subject to the dynamic pressure. *arXiv: Mathematical Physics*.
- RUGGERI, T. & SUGIYAMA, M. 2015 *Rational extended thermodynamics beyond the monatomic gas*. Springer.
- SHARIPOV, F. 2011 Data on the velocity slip and temperature jump on a gas–solid interface. *J. Phys. Chem. Ref. Data* **40** (2), 023101.
- STRUCHTRUP, H. 2005 Derivation of 13 moment equations for rarefied gas flow to second order accuracy for arbitrary interaction potentials. *Multiscale Model. Simul.* **3**, 221–243.
- STRUCHTRUP, H. & NADLER, B. 2020 Are waves with negative spatial damping unstable? *Wave Motion* **97**, 102612.
- STRUCHTRUP, H. & TORRILHON, M. 2003 Regularization of Grad’s 13 moment equations: Derivation and linear analysis. *Phys. Fluids* **15**, 2668–2680.
- STRUCHTRUP, H. & TORRILHON, M. 2008 Higher-order effects in rarefied channel flows. *Phys. Rev. E* **78**, 046301.
- TAKASHI ARIMA, T. R. & SUGIYAMA, M. 2018 Extended thermodynamics of rarefied polyatomic gases: 15-field theory incorporating relaxation processes of molecular rotation and vibration. *Entropy* **20** (4), 301.
- TORRILHON, M. 2016 Modeling nonequilibrium gas flow based on moment equations. *Annu. Rev. Fluid Mech.* **48**, 429–458.
- TORRILHON, M. & STRUCHTRUP, H. 2004 Regularized 13-moment equations: Shock structure calculations and comparison to Burnett models. *J. Fluid Mech.* **513**, 171–198.
- ZHANG, W., MENG, G. & WEI, X. 2012 A review on slip models for gas microflows. *Microfluid Nanofluid* **13**, 845–882.
- ZHDANOV, V. 1968 The kinetic theory of a polyatomic gas. *Soviet Journal of Experimental and Theoretical Physics* **26**, 1187.